International Journal of Thermal Sciences 49 (2010) 993–1002

Contents lists available at ScienceDirect

International Journal of Thermal Sciences

journal homepage: www.elsevier.com/locate/ijts

Heat transfer in micropolar fluid along an inclined permeable plate with variable fluid properties

Mohammad M. Rahman [a,*], A. Aziz [b], Mohamed A. Al-Lawatia [a]

[a] Department of Mathematics and Statistics, College of Science, Sultan Qaboos University, P.O. Box 36, Al-Khod 123, Muscat, Oman
[b] Department of Mechanical Engineering, School of Engineering and Applied Science, Gonzaga University, Spokane, WA 99258, USA

ARTICLE INFO

Article history:
Received 18 October 2009
Received in revised form
1 January 2010
Accepted 1 January 2010
Available online 6 February 2010

Keywords:
Convective flow
Heat transfer
Inclined surface
Locally self-similar solution
Micropolar fluid
Variable electric conductivity
Variable thermal conductivity
Variable viscosity

ABSTRACT

This paper studies the heat transfer process in a two-dimensional steady hydromagnetic natural convective flow of a micropolar fluid over an inclined permeable plate subjected to a constant heat flux condition. The analysis accounts for both temperature dependent viscosity and temperature dependent thermal conductivity. The local similarity equations are derived and solved numerically using the Nachtsheim–Swigert iteration procedure. Results for the dimensionless velocity and temperature profiles and the local rate of heat transfer are displayed graphically delineating the effect of various parameters characterizing the flow. The results show that in modeling the thermal boundary layer flow when both the viscosity and thermal conductivity are temperature dependent, the Prandtl number must be treated as a variable to obtain realistic results. As the thermal conductivity parameter increases, it promotes higher velocities and higher temperatures in the respective boundary layers. The wall shear stress increases with the increase of thermal conductivity parameter. This is true of electrically conducting as well as electrically non-conducting fluids. The presence of heat generation invigorates the flow and produces larger values of the local Nusselt number compared with the case of zero heat generation.

1. Introduction

The micropolar fluids are those which contain micro-constituents and can undergo rotation. These kind of fluids are utilized in analyzing exotic lubricants, the flow of colloidal suspensions, paints, liquid crystals, animal blood, fluid flowing in brain, turbulent shear flows, and body fluids both mathematically and industrially. Since the early studies of Eringen [1,2], many researchers have reported results on micropolar fluids (see [3–16] and the references therein).

The study of variable viscosity thermal boundary layer flow over an isothermal surface is important in processes such as hot rolling, wire drawing, glass fiber production, paper production, gluing of labels on hot bodies, drawing of plastic films, etc. In the classical treatment of thermal boundary layers, the kinematic viscosity is assumed to be constant. However, experimental studies indicate that this assumption is valid only if the temperature variation during the flow is not large. Because many applications involve large temperature variations, numerous researchers have studied flows with temperature dependent viscosity and reported results for both Newtonian and non-Newtonian fluids flowing in different geometries and under various flow conditions (see for example [17–26]).

It is well known that thermo-physical properties of the ambient fluid, especially the thermal conductivity may change with temperature (see [27–31]). Recently, Prasad and Vajravelu [32] have studied the effect of variable thermal conductivity in a non-isothermal sheet stretching through power law fluids. Similar studies for the viscoelastic fluids have been reported by Prasad et al. [33]. Both studies revealed that the effect of variable thermal conductivity is to increase the shear stress.

The thickness of the thermal boundary layer relative to the velocity boundary layer depends on the Prandtl number which by its definition varies directly with the fluid viscosity and inversely with the thermal conductivity of the fluid. As the viscosity and the thermal conductivity vary with temperature so does the Prandtl number. Despite this fact, all of the afore-mentioned studies treated the Prandtl number as a constant. The use of a constant Prandtl number within the boundary layer when the fluid properties are temperature dependent, introduces errors in the computed results. Recently, Rahman and Salahuddin [34] studied hydromagnetic flow of a Newtonian fluid over an inclined plate with variable viscosity whereas Rahman et al. [35] studied the flow of a micropolar fluid with variable viscosity over a permeable stretching sheet. Both

* Corresponding author. Fax: +968 2414 1490.
E-mail address: mansurdu@yahoo.com (M.M. Rahman).

1290-0729/$ – see front matter © 2010 Elsevier Masson SAS. All rights reserved.
doi:10.1016/j.ijthermalsci.2010.01.002

Nomenclature

Roman

B_0	magnetic induction, [Wb m^{-2}]
C_f	local skin-friction coefficient
c_p	specific heat at constant pressure, [kJ kg^{-1} K^{-1}]
f	dimensionless stream function
f_w	dimensionless suction/injection velocity
g_0	acceleration due to gravity, [m s^{-2}]
g	dimensionless microrotation
j	micro-inertia per unit mass, [m^2]
M	local magnetic field parameter
N	microrotation component normal to xy-plane, [s^{-1}]
Nu_x	local Nusselt number
n	microrotation parameter
Pr	variable Prandtl number
Pr_∞	ambient Prandtl number
Q	temperature dependent heat source (or sink) parameter
Q^*	surface dependent heat source (or sink) parameter
q_w	surface heat flux, [W m^{-2}]
q'''	volumetric heat source (or sink), [W m^{-3}]
Re_x	local Reynolds number
S	coefficient of vortex viscosity, [Pa s]
T_w	temperature at the surface of the plate, [K]
T	temperature of the fluid within the boundary layer, [K]
T_∞	temperature of the ambient fluid, [K]
U_∞	free stream velocity, [m s^{-1}]
U_0	characteristic velocity, [m s^{-1}]
v_s	suction/injection velocity, [m s^{-1}]
u, v	the x -and y -component of the velocity field, [m s^{-1}]
x, y	distance along and normal to the plate, [m]

Greek

α	angle of inclination of plate [rad]
β	volumetric coefficient of thermal expansion, [K^{-1}]
λ	local buoyancy parameter
ρ	fluid density, [kg m^{-3}]
ε	thermal conductivity parameter
μ	dynamic viscosity, [Pa s]
μ_∞	dynamic viscosity at ambient temperature, [Pa s]
υ	kinematic viscosity, [m^2 s^{-1}]
υ_∞	kinematic viscosity at ambient temperature, [m^2 s^{-1}]
σ'_0	electrical conductivity of the fluid [S m^{-1}]
σ_0	magnetic permeability [N A^{-2}]
ψ	stream function, [m^2 s^{-1}]
η	similarity variable
θ	dimensionless temperature
θ_r	variable viscosity parameter
κ	thermal conductivity, [Wm^{-1} K^{-1}]
κ_∞	thermal conductivity at ambient temperature, [Wm^{-1} K^{-1}]
Δ	vortex viscosity parameter

Subscripts

w	surface
∞	conditions far away from the surface

studies confirmed that for the accurate prediction of the thermal characteristics of variable viscosity fluid flows, the Prandtl number must be treated as a variable rather than a constant. These studies, however, assumed the thermal conductivity to be a constant. In another study, Rahman et al. [36] investigated the effects of variable electric conductivity and non-uniform heat source (or sink) on convective micropolar fluid flow along an inclined flat plate with a constant surface temperature. They found that the skin-friction coefficient and Nusselt number are higher for the case of constant fluid electric conductivity than for the case of variable fluid electric conductivity. In their model, they treated fluid viscosity and thermal conductivity to be constants.

The objective of the present study is to extend the work of Rahman et al. [36] to a permeable inclined plate and to take into account variable fluid viscosity as well as variable thermal conductivity. Instead of a constant temperature at the plate as in [36], the present paper imposes a constant heat flux condition at the plate. Thus the main focus of the analysis is to investigate how the Prandtl number varies within the boundary layer when both the thermal conductivity and viscosity are temperature dependent and, in addition, there is mass transfer (suction or injection) at the plate. The local similarity equations are derived and solved numerically using the Nachtsheim–Swigert iteration procedure. Graphs and tables are presented to illustrate and discuss important hydrodynamic and thermal features of the flow.

2. Formulation of the problem

2.1. Flow analysis

Consider a steady two-dimensional hydromagnetic laminar convective flow of a viscous, incompressible, micropolar fluid along a semi-infinite inclined impermeable flat plate with an acute angle α to the vertical. The applied magnetic field is assumed to be in the y-direction and varies in strength as a function of x and is defined as:

$$\vec{B} = (0, B(x)). \tag{1}$$

The external electric field is assumed to be zero and the magnetic Reynolds number is assumed to be small. Hence, the induced magnetic field is small compared with the externally applied magnetic field. The fluid of density (ρ) is quiescent $(U_\infty = 0)$ and the convective motion is induced by the buoyancy forces. The viscosity (μ) and thermal conductivity of the fluid (κ) are assumed to be functions of temperature. The pressure gradient, body forces, viscous dissipation and Joule heating effects are neglected compared with the effect of internal heat source (or sink).

Within the framework of the above-noted assumptions, the convective flow of a steady incompressible micropolar fluid subject to the Boussinesq approximation can be described by the following conservation equations (see Rahman et al. [36]):

$$\frac{\partial u}{\partial x} + \frac{\partial v}{\partial y} = 0, \tag{2}$$

$$\rho\left(u\frac{\partial u}{\partial x} + v\frac{\partial u}{\partial y}\right) = \frac{\partial}{\partial y}\left((\mu + S)\frac{\partial u}{\partial y}\right) + S\frac{\partial N}{\partial y} + \rho g_0 \beta (T - T_\infty) \times \cos\alpha - \sigma'_0 (B(x))^2 u, \tag{3}$$

$$\rho j\left(u\frac{\partial N}{\partial x} + v\frac{\partial N}{\partial y}\right) = j\frac{\partial}{\partial y}\left(\left(\mu + \frac{S}{2}\right)\frac{\partial N}{\partial y}\right) - S\left(2N + \frac{\partial u}{\partial y}\right), \tag{4}$$

$$\rho c_p\left(u\frac{\partial T}{\partial x}+v\frac{\partial T}{\partial y}\right) = \frac{\partial}{\partial y}\left(\kappa\frac{\partial T}{\partial y}\right) + q''', \tag{5}$$

where u,v are the velocity components along x,y coordinates, respectively, ρ is the density of the fluid, μ is the dynamic viscosity, S is the microrotation coupling coefficient (also known as the coefficient of gyro-viscosity or the vortex viscosity), N is the microrotation component normal to the xy-plane, j is the micro-inertia per unit mass, T is the temperature of the fluid in the boundary layer, c_p is the specific heat of the fluid at constant pressure, g_0 is the acceleration due to gravity, β is the volumetric coefficient of thermal expansion.

The non-uniform heat source (or sink) q''' (see [37]) is modeled as

$$q''' = \frac{\kappa_\infty U_0}{2\upsilon_\infty x}\left[Q(T-T_\infty)+Q^*(T_w-T_\infty)e^{-\eta}\right], \tag{6}$$

where υ_∞ is the kinematic viscosity at ambient temperature, κ_∞ is the thermal conductivity at ambient temperature, Q and Q^* are the coefficients of space and temperature dependent heat source (or sink) terms, respectively, T_∞ is the ambient temperature, and η is the similarity variable defined later by equation (11). The case of $Q>0$, $Q^*>0$ corresponds to heat generation and that of $Q<0$, $Q^*<0$ corresponds to heat absorption.

For the flow under investigation, the strength of the applied magnetic field $B(x)$ is assumed to be variable and of the form (see Helmy [38]):

$$B(x) = \frac{B_0}{\sqrt{x}}, \text{ where } B_0 \text{ is a constant.} \tag{7}$$

The electrical conductivity σ_0' is assumed to be dependent on the velocity of the fluid and has the following form (see Helmy [38], Aissa and Mohammadein [39], Rahman and Salahuddin [34]).

$$\sigma_0' = \sigma_0 u, \text{ where } \sigma_0 \text{ is a constant.} \tag{8}$$

Using equations (7) and (8), the momentum equation (3) can be written as

$$\rho\left(u\frac{\partial u}{\partial x}+v\frac{\partial u}{\partial y}\right) = \frac{\partial}{\partial y}\left((\mu+S)\frac{\partial u}{\partial y}\right)+S\frac{\partial N}{\partial y}+\rho g_0\beta(T-T_\infty)\times\cos\alpha-\frac{\sigma_0 B_0^2 u^2}{x}. \tag{9}$$

2.2. Boundary conditions

The applicable boundary conditions for the present model are

(i) On the plate surface ($y=0$):

$$u=0,\ v=\pm v_s \text{ (no}-\text{slip and permeable wall conditions)} \tag{10a}$$

$$N=-n\frac{\partial u}{\partial y} \text{ (microrotation proportional to vorticity)} \tag{10b}$$

$$\frac{\partial T}{\partial y}=-\frac{q_w}{\kappa_\infty} \text{ (uniform surface heat flux)} \tag{10c}$$

(ii) Matching with the quiescent free stream ($y\to\infty$):

$$u=U_\infty=0,\ N=0,\ T=T_\infty, \tag{10d}$$

where the subscripts w and ∞ refer to the wall and boundary layer edge, respectively. A linear relationship between the microrotation function N and the surface shear $\partial u/\partial y$ is chosen for investigating the effect of different surface conditions for microrotation. When microrotation parameter $n=0$, we obtain $N=0$ which represents no-spin condition i.e. the microelements in a concentrated particle flow-close to the wall are not able to rotate as stipulated by Jena and Mathur [40]. The case $n=0.5$ represents vanishing of the anti-symmetric part of the stress tensor and represents weak concentration. For this case, Ahmadi [41] suggested that in a fine particle suspension, the particle spin is equal to the fluid velocity at the wall. The case of $n=1$ is representative of the turbulent boundary layer flows (see Peddison and McNitt [42]).

2.3. Introduction of dimensionless variables

We introduce the following dimensionless variables:

$$\eta = y\sqrt{\frac{U_0}{2\upsilon_\infty x}},\ \psi=\sqrt{2\upsilon_\infty U_0 x}f(\eta),\ N=\sqrt{\frac{U_0^3}{2\upsilon_\infty x}}g,\quad \theta(\eta)=\frac{T-T_\infty}{T_w-T_\infty}, \tag{11}$$

where ψ is the stream function, U_0 is some reference velocity, and

$$T_w-T_\infty = q_w/k_\infty\sqrt{2\upsilon_\infty x/U_0}.$$

Since $u=\partial\psi/\partial y$ and $v=-\partial\psi/\partial x$ we have from equation (11)

$$u=U_0 f' \text{ and } v=-\sqrt{\frac{\upsilon_\infty U_0}{2x}}(f-\eta f'), \tag{12}$$

where f is non-dimensional stream function and prime denotes differentiation with respect to η.

With the increase of temperature, the fluid viscosity in the momentum boundary layer decreases which in turn affects the heat transfer rate at the wall. Thus in order to predict the flow and heat transfer rates accurately, it is necessary to take into account the temperature dependence of the fluid viscosity. Ling and Dybbs [43] suggest a temperature dependent viscosity of the form

$$\frac{1}{\mu}=\frac{1}{\mu_\infty}[1+\gamma(T-T_\infty)], \tag{13}$$

where γ is the thermal property of the fluid. Equation (13) can be rewritten as

$$\frac{1}{\mu}=A(T-T_r), \tag{14}$$

where,

$$A=\frac{\gamma}{\mu_\infty} \text{ and } T_r=T_\infty-\frac{1}{\gamma}. \tag{15}$$

In the above relations (15), both A and T_r are constants and their values depend on the reference state land γ. For liquids, $A>0$ and for gases, $A<0$. Typical values of γ and A for air are $\gamma=0.026240$ and $A=-123.2$ (see Weast [44]). The dimensionless temperature θ can also be written as

$$\theta=\frac{T-T_r}{T_w-T_\infty}+\theta_r, \tag{16}$$

where $\theta_r=T_r-T_\infty/T_w-T_\infty=-1/\gamma(T_w-T_\infty)$ and its value is determined by the viscosity/temperature characteristics of the fluid under consideration and the temperature difference T_w-T_∞. Using (16), equation (13) becomes

$$\mu = \mu_\infty \left(\frac{\theta_r}{\theta_r - \theta}\right). \tag{17}$$

The variation of viscosity with temperature represented by equations (14) and (17) has been used by numerous researchers. Other models such as the Reynolds and Vogel's viscosity models have also been used in the literature. Knezevic and Savic [45] investigated in detail the applicability of the Reynolds viscosity model and found that this model is accurate only for a very limited temperature range. On the other hand, Vogel's viscosity model is usually used for modeling thermal boundary layers in third-grade fluids (see Yurusoy and Pakdemirli [46]). The viscosity model considered in the present paper is more appropriate for the present study than the Reynolds and Vogel's viscosity models because it is valid for a wider range of temperatures.

Savvas et al. [47] observed that for liquid metals, the thermal conductivity varies linearly with temperature in the range 0–400 °F. We follow Savvas et al. [47] and assume the thermal conductivity of the fluid to be a linear function of the temperature. The specific model used is (see Chiam [27])

$$\kappa = \kappa_\infty \left(1 + \varepsilon \frac{T - T_\infty}{\Delta T}\right), \tag{18}$$

where ε is the thermal conductivity parameter and $\Delta T = T_w - T_\infty$.

Now introducing equations (11),(12),(17) and (18) into equations (4),(5) and (9), we obtain,

$$\left(\frac{\theta_r}{\theta_r - \theta} + \Delta\right) f''' + ff'' + \frac{\theta_r}{(\theta_r - \theta)^2} f''\theta' + \Delta g' + \lambda\theta\cos\alpha - Mf'^2 = 0, \tag{19}$$

$$\left(\frac{\theta_r}{\theta_r - \theta} + \frac{1}{2}\Delta\right) g'' - 2\Delta(2g + f'') + f'g + fg' + \frac{\theta_r}{(\theta_r - \theta)^2} g'\theta' = 0, \tag{20}$$

$$(1 + \varepsilon\theta)\theta'' + \varepsilon\theta'^2 + \Pr_\infty (f\theta' - f'\theta) + (Q\theta + Q^* e^{-\eta}) = 0, \tag{21}$$

where

$\Delta = S/\mu_\infty$ is the vortex viscosity parameter, $j = \upsilon_\infty x/U_0$ is the micro-inertia per unit mass, $\lambda = 2g_0\beta x(T_w - T_\infty)/U_0^2$ is the buoyancy parameter, $M = 2\sigma_0 B_0^2/\rho$ is the magnetic field parameter and $\Pr_\infty = \mu_\infty c_p/k_\infty$ is the ambient Prandtl number.

The corresponding boundary conditions (10) become,

$$\left.\begin{array}{l} f = f_w, f' = 0, g = -nf'', \theta' = -1 \text{ at } \eta = 0, \\ f' = 0, g = 0, \theta = 0 \text{ as } \eta \to \infty, \end{array}\right\} \tag{22}$$

where $f_w = -\upsilon_s(2x/\upsilon_\infty U_0)^{1/2}$ represents suction/injection velocity at the plate for $\upsilon_s < 0$ and $\upsilon_s > 0$, respectively.

2.4. Variable Prandtl number

The definition of Prandtl number shows that it is a function of viscosity, thermal conductivity and specific heat. Because both viscosity and thermal conductivity vary across the boundary layer, the Prandtl number also varies. The assumption of constant Prandtl number inside the boundary layer when the viscosity and the thermal conductivity are temperature dependent leads to unrealistic results (see Pantokratoras [48,49], Rahman and Salahuddin [34], and Rahman et al. [35]). In the present work, the Prandtl number is defined as

$$\Pr = \frac{\mu c_p}{\kappa} = \frac{\left(\frac{\theta_r}{\theta_r - \theta}\right)\mu_\infty c_p}{\kappa_\infty(1 + \varepsilon\theta)} = \frac{1}{\left(1 - \frac{\theta}{\theta_r}\right)(1 + \varepsilon\theta)} \Pr_\infty. \tag{23}$$

With the use of equation (23), the non-dimensional temperature equation (21) can be expressed as

$$(1 + \varepsilon\theta)\theta'' + \varepsilon\theta'^2 + \Pr\left(1 - \frac{\theta}{\theta_r}\right)(1 + \varepsilon\theta)(f\theta' - f'\theta) + (Q\theta + Q^* e^{-\eta}) = 0. \tag{24}$$

From equation (23) it can be seen that for large θ_r i.e. $\theta_r \to \infty$ and small ε i.e. $\varepsilon \to 0$, the variable Prandtl number Pr equals to the ambient Prandtl number $\Pr_\infty$, in that case equation (24) reduces to the equation (21). For $\eta \to \infty$, $\theta(\eta)$ becomes zero and therefore $\Pr = \Pr_\infty$ regardless of the values of θ_r and ε. Equation (24) is the corrected non-dimensional form of the energy equation in which Prandtl number is treated as variable. To the best of our knowledge, nobody has incorporated this correction into the non-dimensional energy equation (24) for modeling the thermal boundary layer flows with temperature dependent viscosity and thermal conductivity.

2.5. Skin-friction coefficient and Nusselt number

The quantities of engineering interest are the skin-friction coefficient (rate of shear stress) and the Nusselt number (rate of heat transfer). The local skin-friction coefficient is defined as

$$C_f = \sqrt{\frac{2}{\mathrm{Re}_x}}\left[\left(\frac{\theta_r}{\theta_r - \theta(0)}\right) + (1 - n)\Delta\right] f''(0), \tag{25}$$

or,

$$C_f^* = f''(0) \text{ where } C_f^* = \sqrt{\frac{\mathrm{Re}_x}{2}}\, \frac{C_f}{\left[\left(\frac{\theta_r}{\theta_r - \theta(0)}\right) + (1 - n)\Delta\right]}. \tag{26}$$

The local Nusselt number is given by

$$Nu_x = \left(2^{-1}\mathrm{Re}_x\right)^{\frac{1}{2}} \frac{1}{\theta(0)}, \tag{27}$$

or,

$$Nu_x^* = \theta(0) \text{ where } Nu_x^* = \sqrt{2}\mathrm{Re}^{\frac{-1}{2}} \frac{1}{Nu_x}. \tag{28}$$

The numerical values of C_f^* and Nu_x^* are calculated from equations (26) and (28), respectively.

3. Numerical solutions

The set of equations (19), (20) and (24) is highly nonlinear and coupled and therefore it cannot be solved analytically. The nonlinear system consisting of equations (19), (20) and (24) with boundary conditions (22) are solved using the Nachtsheim–Swigert [50] shooting iteration technique. The method is well established and has been successfully implemented to study a variety of nonlinear heat and fluid flow problems. Adopting this numerical technique, a computer program was written for the solution of these equations incorporating a sixth-order Runge-Kutta integration scheme.

In order to verify the effect of the integration step size $\Delta\eta$, the code was run with three different step sizes namely; $\Delta\eta = 0.005$, $\Delta\eta = 0.003$ and $\Delta\eta = 0.001$. In each case, the numerical results exhibited excellent consistency. It was found that $\Delta\eta = 0.001$

provided sufficiently accurate (error less than 10^{-6}) results and further refinement of the grid size was therefore not warranted.

4. Results and discussion

For the purpose of discussion, the numerical results are presented in the form of non-dimensional velocity and temperature profiles. Parametric studies were conducted by varying the thermal conductivity parameter ε, variable viscosity parameter θ_r, and suction/injection parameter f_w. The choice of the values of the parameters was dictated by the values chosen by the previous investigators. Because of the lack of experimental data for vortex viscosity parameter, suitable representative value was chosen in order to determine the polar effects on the flow characteristics. Since we are considering a free convection cooling situation, only positive large values of λ are chosen. In the simulations the default values of the parameters are considered as $\Delta = 2.0$, $\varepsilon = 0.2$, $\theta_r = 5.0$, $f_w = 0.5$, $\lambda = 20.0$, $M = 0.5$, $Q = Q^* = 0.5$, and $\mathrm{Pr} = 1.0$ unless otherwise specified. It may be noted that for $\varepsilon = 0$, $\theta_r \to \infty$, and $f_w = 0$, the present problem reduces to that of Rahman et al. [36].

The effect of thermal conductivity parameter ε on the velocity distribution is illustrated in Fig. 1 for $\varepsilon = 0$, 0.5, 1.0, 1.5, and 2.0. The corresponding temperature profiles appear in Fig. 2. The curve marked $\varepsilon = 0$ represents the case of constant fluid thermal conductivity. As ε increases, i.e. as the thermal conductivity increases with temperature, both the velocity and temperature in the respective boundary layers increase. The peak velocity increases by about 7% as ε increases from 0 to 1, while the corresponding increase in the peak temperature is about 6%. Because a constant surface heat flux is imposed at the plate, the maximum temperature occurs at the surface of the plate and decreases away from the plate.

Fig. 3(a) shows the effect of positive values of the viscosity parameter θ_r on the velocity profiles. The effect of increase θ_r is to increase the velocity for $\eta < 0.6$. However, beyond this range, the velocity profiles overlap and the trend is reversed, that is, the velocity decreases with the increase of θ_r. At $\eta = 3.2$, the distinction between the curves disappears. For very large values of $\theta_r (\to \infty)$, the effect of $\theta_r$on the velocity profile is minimal. This is due to the fact that as $\theta_r \to \infty$ the factor $\theta_r/\theta_r - \theta$ in equation (17) approaches

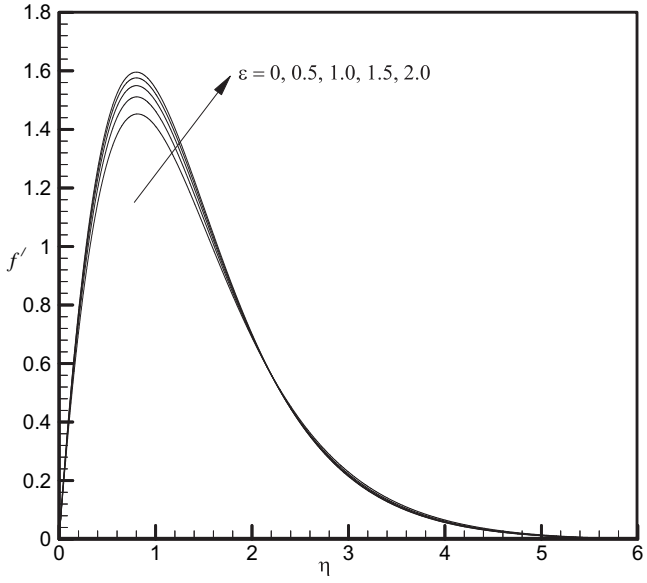

Fig. 1. Velocity profile versus η for different values of ε.

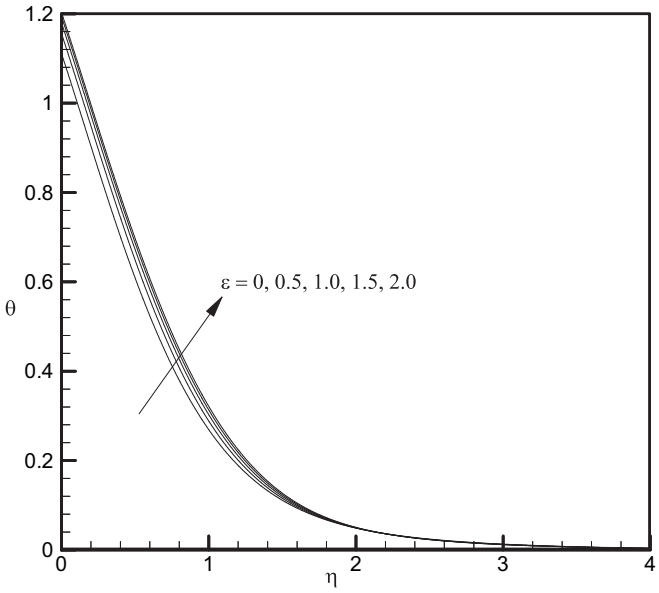

Fig. 2. Temperature profile versus η for different values of ε.

its limiting value of 1 as $\mu = \mu_\infty$. In the numerical simulations, the condition $\theta_r \to \infty$ was achieved by setting $1/\theta_r = 0$. Fig. 3(b) shows the effect of negative values of θ_r on the velocity profiles. In the range $0 \le \eta \le 2.5$, the velocity is seen to increase sharply with the increase in the negative value of θ_r. For $\eta > 2.5$, the velocity profiles overlap and the velocity now decreases as the negative value of θ_r increases.

The temperature profiles for positive and negative values of the viscosity parameter θ_r are plotted in Fig. 4(a) and (b), respectively. Fig. 4(a) shows that as θ_r increases, the thickness of the boundary layer decreases with a consequent reduction of the temperature in the boundary layer. For negative values of θ_r, the trend is reversed. As the negative value of θ_r increases from 0.05 to 100, the boundary layer gradually thickens accompanied by progressively higher temperature.

The effects of the suction/injection parameter f_w, on the velocity profile for a strongly buoyant flow is shown in Fig. 5 for two cases: (1) constant thermal conductivity (ε=0) and constant viscosity ($\theta_r = \infty$) and (2) temperature dependent thermal conductivity (ε=0.2) and temperature dependent viscosity ($\theta_r = 5$). In both cases, the velocity decreases as the mass transfer process at the plate goes from injection ($f_w = -2$) to suction ($f_w = 2$). In both cases, the location of the peak velocity shifts closer to the plate surface as f_w increases. Also, as f_w increases, the thickness of the boundary layer decreases. The effect of variable properties (solid lines) is to promote higher velocities compared with those generated with constant-property flow model (dashed lines).

Fig. 6 depicts the temperature profiles across the boundary layer for various values of f_w for both the cases of constant and variable fluid properties. As f_w increases from injection ($f_w = -2$) to suction ($f_w = 2$), the effect is to lower the temperature levels in the thermal boundary layer. For each value of f_w selected for the numerical computations, the variable-property model yielded higher temperatures (solid lines) compared with the constant-property model (dashed lines). The results of Figs. 5 and 6 clearly show that the wall transpiration (injection or suction) provides an effective means of controlling the flow and heat transfer characteristics.

Equation (23) was used to compute the variation of Pr_∞ within the boundary layer for various values of $\theta_r$with $Pr = 1.0$. The results are shown in Fig. 7(a) for positive values of θ_r and in Fig. 7(b)

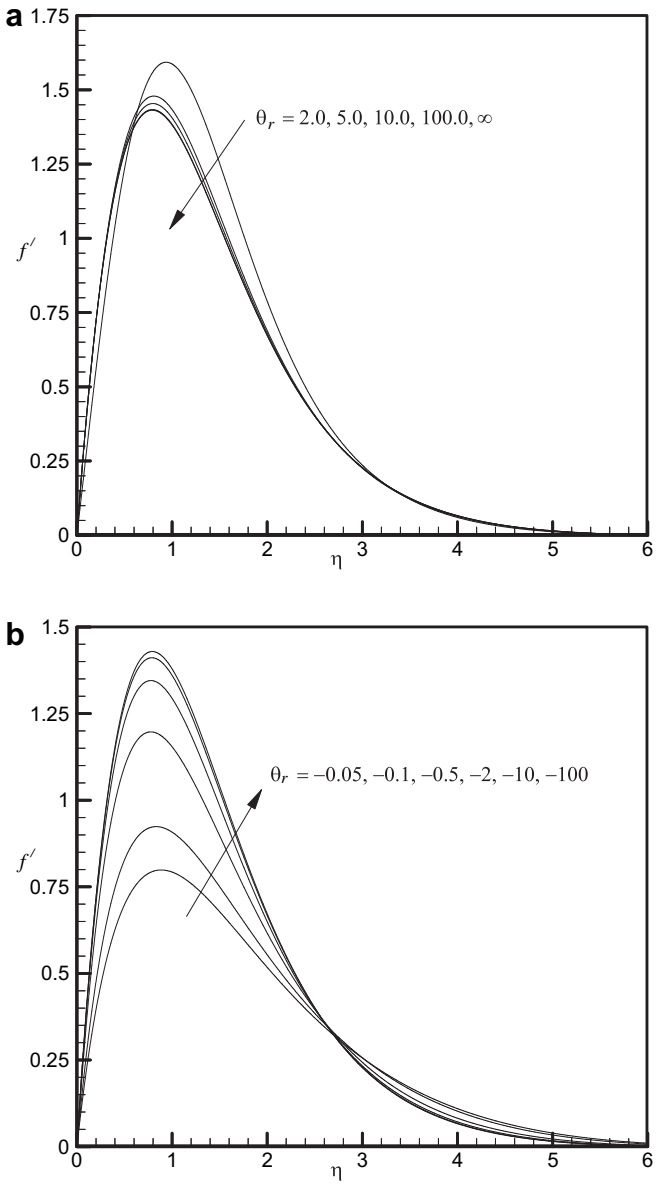

Fig. 3. (a) Velocity profile versus η for different values of $\theta_r(>0)$. (b) Velocity profile versus η for different values of $\theta_r(<0)$.

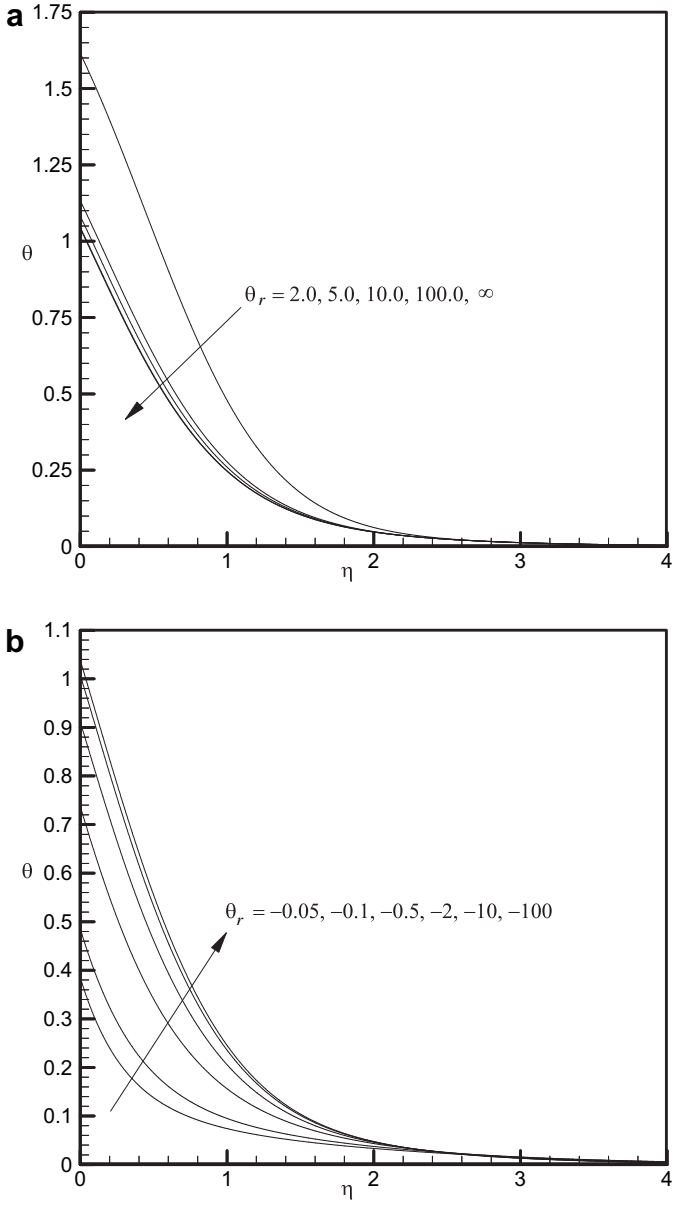

Fig. 4. (a) Temperature profile versus η for different values of $\theta_r(>0)$. (b) Temperature profile versus η for different values of $\theta_r(<0)$.

for negative values of θ_r. Three points emerging from Fig. 7(a) are worth noting. First, the ambient Prandtl number, Pr_∞, asymptotically converges to the value of Pr as $\eta\to\infty$ as it should. Second, for $\theta_r > 0$, the ambient Prandtl number, Pr_∞, increases as θ_r increases. Third, for large values of θ_r, the ambient Prandtl number at the surface of the plate approaches the value of 1, i.e.Pr_∞ at $\eta = 0$ nearly equals Pr. Fig. 7(b) also manifests three worth noting features. First, the ambient Prandtl number Pr_∞, asymptotically converges to the value of Pr as $\eta\to\infty$ as it should. Second, as the negative value of θ_r increases, the ambient Prandtl number, Pr_∞, also decreases. Third, for large negative values of θ_r, the ambient Prandtl number at the surface of the plate approaches the value of 1, i.e. Pr_∞ at $\eta = 0$ nearly equals Pr.

Fig. 8 illustrates the effect of thermal conductivity parameter; ε on the variation of the ambient Prandtl number Pr_∞, with η for $Pr = 1.0$. Like Fig. 7(a) and (b), Fig. 8 also correctly exhibits the asymptotic behavior of Pr_∞, that is, $Pr_\infty = Pr$ as $\eta\to\infty$. As ε increases, the ambient Prandtl number increases significantly. The largest increase occurs at the surface of the plate where Pr_∞ increases from a value of 0.8 for $\varepsilon = 0$ to 2.6 for $\varepsilon = 2$, a factor of more than three.

The variation of Pr_∞ with η at $Pr = 1.0$ is displayed for various values of the suction/injection parameter f_w in Fig. 9. Compared with the case of zero mass transfer, the ambient Prandtl number at the surface of the plate decreases as suction intensifies while an opposite behavior is with the strengthening of injection. Figs. 7–9 clearly establish that the Prandtl number varies significantly within the boundary layer when the fluid properties vary with temperature. Thus, in modeling the flow of fluids with variable properties, the Prandtl number cannot be taken as a constant.

Tables 1–3 present the wall shear stress which is proportional to $f''(0)$ and the wall temperature, $\theta(0)$. Table 1 shows the effect of f_w on the shear stress and the wall temperature. As the parameter f_w increases, the wall shear stress decreases. This is true irrespective of

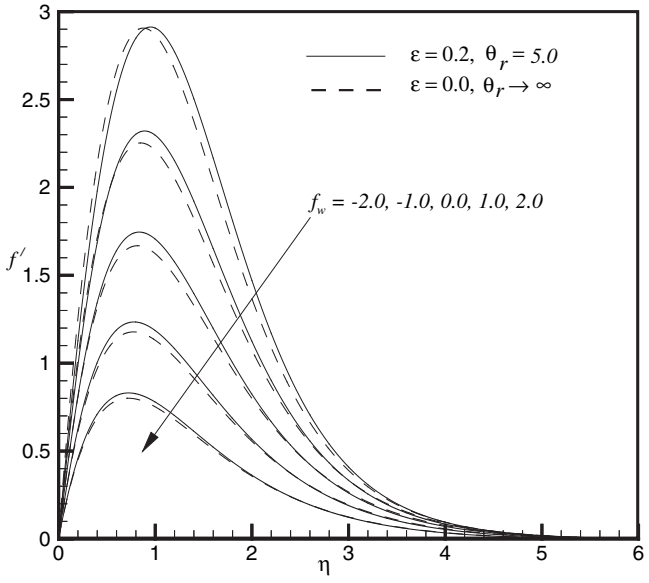

Fig. 5. Velocity profile versus η for different values of f_w.

whether heat generation and the magnetic field are present or absent. Comparison of results for $f''(0)$ in the third and fifth columns shows that for the same M (=0.5), the presence of heat generation ($Q = Q^* = 0.5$) produces higher shear stress than when the heat generation is absent ($Q = Q^* = 0$). The effect of magnetic field on the shear stress may be assessed by comparing the results of $f''(0)$ in fourth and fifth columns. For the same heat generation ($Q = Q^* = 0.5$), the increase in magnetic field parameter M from 0 (non-conducting fluid) to 0.5 (electrically conducting fluid) reduces the shear stress. This can be explained as follows; for $M = 0$, the hydromagnetic term, $-Mf'2$, in Eq. (19) vanishes leading to higher flow velocities compared to the case of electrically conducting fluids ($M \neq 0$). Thus as M increases, the effect is to reduce the shear stress. The conclusions regarding the effects of heat generation and magnetic field on shear stress hold true for all values of suction/injection parameter f_w considered.

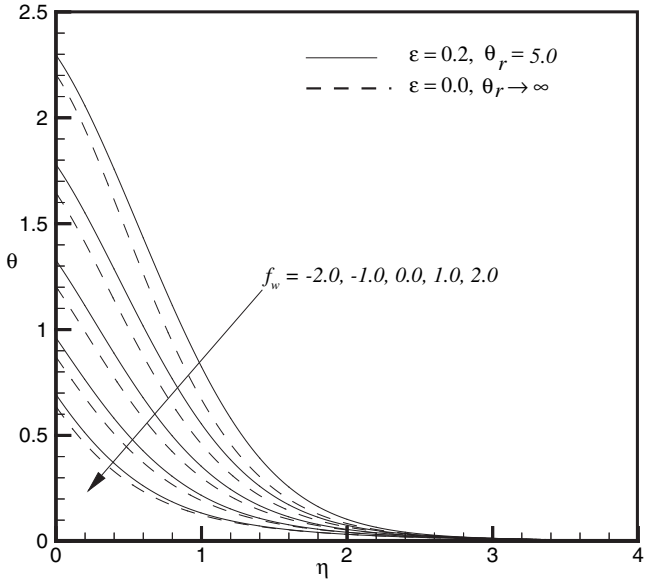

Fig. 6. Temperature profile versus η for different values of f_w.

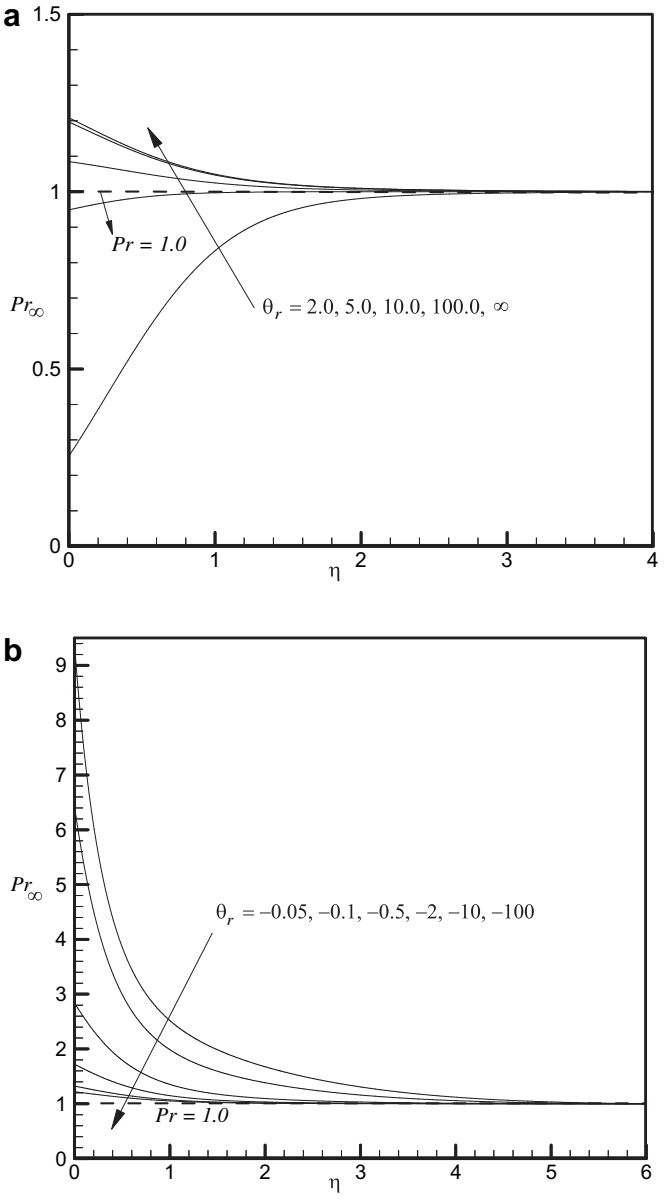

Fig. 7. (a) Ambient Prandtl number versus η for different values of $\theta_r(> 0)$. (b) Ambient Prandtl number versus η for different values of $\theta_r(< 0)$.

Table 1 also shows that the value of Nu_x^* decrease as the parameter f_w increases whether heat generation and magnetic field are present or absent. For a given f_w (suction or injection), the presence of heat generation produces larger values of Nu_x^* compared with the corresponding values for no heat generation. For a given f_w (suction or injection), and heat generation, the presence of magnetic field produces larger values of Nu_x^* compared with the values when the magnetic field is absent.

Table 2 illustrates the effect of thermal conductivity parameter; ε on the shear stress and the Nusselt number. The shear stress increases with the increase of thermal conductivity parameter; ε for both cases of electrically conducting ($M \neq 0$) and non-conducting ($M = 0$) fluids. With analogy to Table 1, the presence of heat generation increases the shear stress. Further, the shear stress values are larger for a non-conducting fluid than that for conducting fluid. It is also noticed that the shear stress for the variable thermal conductivity case is higher than that for the constant

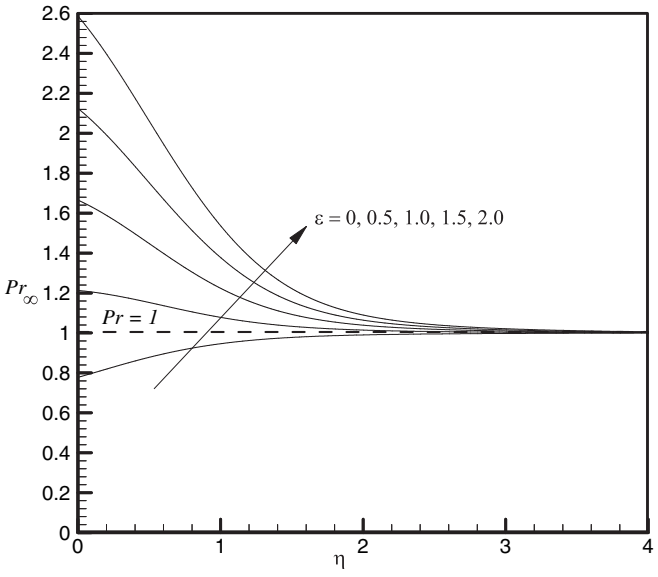

Fig. 8. Ambient Prandtl number versus η for different values of ε.

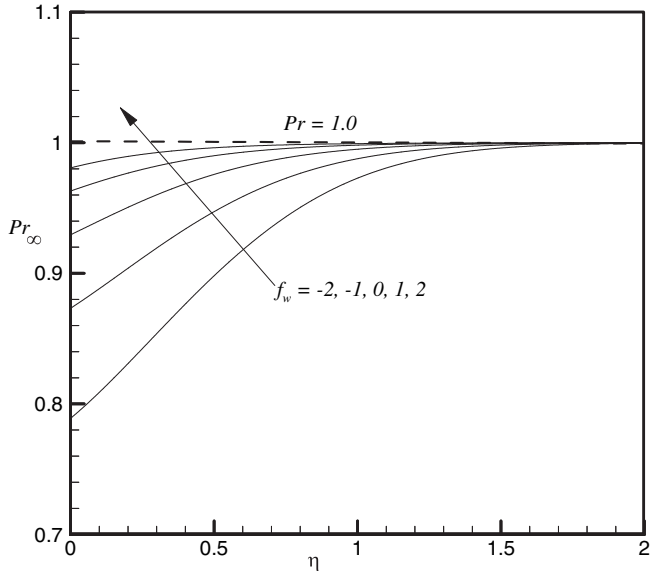

Fig. 9. Ambient Prandtl number versus η for different values of f_w.

Table 1
Values of $C_f^* = f''(0)$ and $Nu_x^* = \theta(0)$ for various values of f_w and $\Delta = 2.0, \varepsilon = 0.2$, $\theta_r = 5.0$, $\lambda = 20.0$, Pr = 1.0, $n = 0.5$, $\alpha = 30^\circ$.

f_w	Values of	$Q = Q^* = 0$, $M = 0.5$	$Q = Q^* = 0.5$, $M = 0$	$Q = Q^* = 0.5$, $M = 0.5$
−2.0	$f''(0)$	5.367952	6.524205	6.318658
−2.0	$\theta(0)$	1.836684	2.168744	2.296969
−1.0	$f''(0)$	4.645779	5.851180	5.681020
−1.0	$\theta(0)$	1.406378	1.694331	1.780061
0.0	$f''(0)$	3.709962	4.956512	4.811868
0.0	$\theta(0)$	1.026503	1.278722	1.327555
1.0	$f''(0)$	2.648817	3.959507	3.840565
1.0	$\theta(0)$	0.718203	0.939526	0.961766
2.0	$f''(0)$	1.639195	3.018178	2.932432
2.0	$\theta(0)$	0.493076	0.686277	0.694082

Table 2
Values of $C_f^* = f''(0)$ and $Nu_x^* = \theta(0)$ for various values of ε and $\Delta = 2.0, f_w = 0.5$, $\theta_r = 5.0$, $\lambda = 20.0$, Pr = 1.0, $n = 0.5$, $\alpha = 30^\circ$.

ε	Values of	$Q = Q^* = 0$, $M = 0.5$	$Q = Q^* = 0.5$, $M = 0$	$Q = Q^* = 0.5$, $M = 0.5$
0.0	$f''(0)$	3.011372	4.370857	4.245006
0.0	$\theta(0)$	0.816164	1.076655	1.110946
0.2	$f''(0)$	3.186506	4.461049	4.328751
0.2	$\theta(0)$	0.862391	1.098689	1.132665
0.5	$f''(0)$	3.417152	4.565945	4.424700
0.5	$\theta(0)$	0.921839	1.122612	1.155870
1.0	$f''(0)$	3.713898	4.686349	4.532523
1.0	$\theta(0)$	0.995650	1.147628	1.179802
1.5	$f''(0)$	3.923578	4.766293	4.602687
1.5	$\theta(0)$	1.045664	1.162582	1.193972
2.0	$f''(0)$	4.074711	4.822515	4.651781
2.0	$\theta(0)$	1.080368	1.172352	1.203088

thermal conductivity even when the fluid viscosity is variable. It may be remarked from the table that Nu_x^* increases with the increase of ε for both conducting and non-conducting fluids whether internal heat generation is present or absent.

Finally, Table 3 illustrates the effect of viscosity parameter θ_r on the shear stress and Nusselt number. For $\theta_r > 0$, the shear stress increases as θ_r increases. This is true for both conducting and non-conducting fluids as well as whether the heat generation is present or absent. For non-conducting fluids the shear stress is higher compared with that for the conducting fluids. In conducting fluids, internal heat generation produces larger values of the shear stress than its absence for all increasing values of $\theta_r > 2$ (not precisely

Table 3
Values of $C_f^* = f''(0)$ and $Nu_x^* = \theta(0)$ for various values of θ_r and $\Delta = 2.0, f_w = 0.5$, $\varepsilon = 0.2$, $\lambda = 20.0$, Pr = 1.0, $n = 0.5$, $\alpha = 30^\circ$.

θ_r	Values of	$Q = Q^* = 0$, $M = 0.5$	$Q = Q^* = 0.5$, $M = 0$	$Q = Q^* = 0.5$, $M = 0.5$
1.99	$f''(0)$	2.893249	3.288916	2.773580
1.99	$\theta(0)$	0.965325	1.471357	1.618746
2	$f''(0)$	2.893729	3.294244	2.790752
2	$\theta(0)$	0.965202	1.470146	1.614978
2.01	$f''(0)$	2.898470	3.344245	2.924450
2.01	$\theta(0)$	0.963979	1.458710	1.585259
3	$f''(0)$	3.105118	4.285974	4.158284
3	$\theta(0)$	0.899817	1.187756	1.229627
4	$f''(0)$	3.161571	4.413277	4.283679
4	$\theta(0)$	0.875379	1.127481	1.163764
5	$f''(0)$	3.186506	4.461049	4.328751
5	$\theta(0)$	0.862391	1.098689	1.132665
10	$f''(0)$	3.222137	4.520489	4.381996
10	$\theta(0)$	0.839294	1.051333	1.081927
100	$f''(0)$	3.242522	4.547930	4.404131
100	$\theta(0)$	0.821076	1.016773	1.045132
∞	$f''(0)$	3.244235	4.549939	4.405579
∞	$\theta(0)$	0.819179	1.013286	1.041429
−0.05	$f''(0)$	1.799030	2.649515	2.498723
−0.05	$\theta(0)$	0.345752	0.380798	0.385124
−0.1	$f''(0)$	2.260927	3.192630	3.022758
−0.1	$\theta(0)$	0.431360	0.478697	0.485356
−0.5	$f''(0)$	3.056077	4.206696	4.023540
−0.5	$\theta(0)$	0.628393	0.722475	0.736860
−1.0	$f''(0)$	3.200143	4.427162	4.252408
−1.0	$\theta(0)$	0.695783	0.815622	0.833691
−2.0	$f''(0)$	3.253886	4.528720	4.363907
−2.0	$\theta(0)$	0.745501	0.889742	0.911201
−5.0	$f''(0)$	3.262324	4.562584	4.408294
−5.0	$\theta(0)$	0.785421	0.954097	0.978838
−10.0	$f''(0)$	3.256688	4.561709	4.412309
−10.0	$\theta(0)$	0.801386	0.981468	1.007687
−100.0	$f''(0)$	3.245855	4.551775	4.406861
−100.0	$\theta(0)$	0.817305	1.009859	1.037793

determined). An opposite trend is observed for some $\theta_{rcrit} < \theta_r \leq 2$. From equation (25) we see that value of θ_r cannot be equal to $\theta(0)$ (an unknown surface boundary condition for the temperature field). Thus, it is worth mentioning that for $\theta_r \in (0, \theta(0))$ no solutions could be found. For negative values of $\theta_r (< 0)$, shear stress increases with the increase of absolute value of θ_r up to a certain limit of absolute value of θ_r. Beyond this limit of θ_r shear stress decreases with the further increase of absolute value of θ_r. It is also important to note that for $\theta_r (< 0)$, values of Nu_x^* decrease with the increase of absolute value of θ_r for both conducting and non-conducting fluids.

5. Conclusions

A mathematical model has been developed for the hydromagnetic natural convection boundary layer flow of a micropolar fluid under an inclined permeable plate with temperature dependent fluid viscosity and thermal conductivity as well as with variable fluid electric conductivity. The dimensionless conservation equations have been solved numerically using Nachetsheim–Swigert iteration technique with a sixth-order Runge–Kutta integration method. The numerical computations have led to the following conclusions:

i) An increase in wall suction impedes the flow and pushes the peak velocity in the velocity boundary layer closer to the plate surface. The effect of varying the fluid properties (viscosity and thermal conductivity) is to promote higher velocities compared to those generated with constant properties fluid.
ii) An increase in suction reduces the temperature level throughout the thermal boundary layer. The effect of variable properties is to increase the temperature compared to the case of constant properties fluid.
iii) The effect of injection is to increase the velocity and temperature profiles in the respective boundary layers. Thus the effect of injection is opposite to that of suction.
iv) The peak velocity moves close to the surface of the plate with the increase of the fluid variable viscosity parameter when $\theta_r > 0$, while an opposite effect is observed when $\theta_r < 0$.
v) For $\theta_r > 0$, an increase in θ_r leads to a decrease in the thermal boundary layer thickness while for $\theta_r < 0$, an increase in θ_r increases the thickness of the thermal boundary layer.
vi) The ambient Prandtl number varies throughout the thermal boundary when the injection/suction parameter or the thermal conductivity parameter or the viscosity parameter is each allowed to vary.
vii) For modeling thermal boundary layers with temperature dependent viscosity and thermal conductivity, the Prandtl number must be treated as a variable inside the boundary layer.
viii) The wall shear stress increases with the increase in the thermal conductivity parameter for both electrically conducting ($M \neq 0$) and non-conducting ($M = 0$) fluids.
ix) The wall shear stress is higher for a non-conducting fluid than for a conducting fluid.
x) The effect of a magnetic field on the shear stress is similar to that due to suction.

References

[1] A.C. Eringen, Theory of micropolar fluids. J. Math. Mech. 16 (1966) 1–18.
[2] A.C. Eringen, Theory of thermomicropolar fluids. J. Math. Anal. Appl. 38 (1972) 480–496.
[3] G. Ahmadi, Self-similar solution of incompressible micropolar boundary layer flow over a semi-infinite plate. Int. J. Eng. Sci. 14 (1976) 639–646.
[4] S.K. Jena, M.N. Mathur, Similarity solution for laminar free convection flow of thermomicropolar fluid past a non-isothermal vertical flat plate. Int. J. Eng. Sci. 19 (1981) 1431–1439.
[5] R.S.R. Gorla, H.S. Takhar, Free convection boundary layer flow of a micropolar fluid past slender bodies. Int. J. Eng. Sci. 25 (1987) 949–962.
[6] R.S.R. Gorla, Combined forced and free convection in micropolar boundary layer flow a vertical flat plate. Int. J. Eng. Sci. 26 (1988) 385–391.
[7] A. Yucel, Mixed convection micropolar fluid flow over horizontal plate with surface mass transfer. Int. J. Eng. Sci. 27 (1989) 1593–1608.
[8] R.S.R. Gorla, P.P. Lin, A.J. Yang, Asymptotic boundary layer solutions for mixed convection from a vertical surface in a micropolar fluid. Int. J. Eng. Sci. 28 (1990) 525–533.
[9] R.S.R. Gorla, Mixed convection in a micropolar fluid from a vertical surface with uniform heat flux. Int. J. Eng. Sci. 30 (1992) 349–358.
[10] M.A. Hossain, M.K. Chaudhury, Mixed convection flow of a micropolar fluid over an isothermal plate with variable spin gradient viscosity. Acta Mech. 131 (1998) 139–151.
[11] D.A.S. Rees, I. Pop, Free convection boundary layer flow of micropolar fluid from a vertical flat plat. IMAJ. Appl. Math. 61 (1998) 179–197.
[12] M.M. Rahman, M.A. Sattar, Magnetohydrodynamic convective flow of a micropolar fluid past a continuously moving vertical porous plate in the presence of heat generation/absorption. ASME J. Heat Transfer 128 (2006) 142–152.
[13] M.M. Rahman, M.A. Sattar, Transient convective flow of micropolar fluid past a continuously moving vertical porous plate in the presence of radiation. Int. J. App. Mech. Egn 12 (2007) 497–513.
[14] M.M. Rahman, T. Sultana, Radiative heat transfer flow of micropolar fluid with variable heat flux in a porous medium. Nonlinear Anal. Model. Control 13 (2008) 71–87.
[15] M.M. Rahman, Convective flows of micropolar fluids from radiate isothermal porous surfaces with viscous dissipation and joule heating. Commun. Nonlinear. Sci. Numer. Simulat. 14 (2009) 3018–3030.
[16] M.M. Rahman, I.A. Eltayeb, S.M.M. Rahman, Thermo-micropolar fluid flow along a vertical permeable plate with uniform surface heat flux in the presence of heat generation. Thermal Sci. 13 (2009) 23–36.
[17] H. Herwig, G. Wickern, The effect of variable properties on laminar boundary layer flow. Wärme und Stoffübertragung 20 (1986) 47–57.
[18] O.D. Makinde, Heat and mass transfer in a pipe with moving surface effect of viscosity variation and energy dissipation. Quaestion. Math. 24 (2001) 93–104.
[19] A.Z. Szeri, K.R. Rajagopal, Flow of a non-Newtonian fluid between heated parallel plates. Int. J. Non-Linear Mech. 20 (1985) 91–101.
[20] M. Yürüsoy, M. Pakdemirli, B.S. Yilbaş, Perturbation solution for a third-grade fluid flowing between parallel plates. Proc. IMechE, Part C: J. Mech. Eng. Sci. 222 (2008) 653–656.
[21] E. Ali, The effect of variable viscosity on mixed convection heat transfer along a vertical moving surface. Int. J. Thermal Sci. 45 (2006) 60–69.
[22] O.D. Makinde, Laminar falling liquid film with variable viscosity along an inclined heated plate. App. Math. Comp. 175 (2006) 80–88.
[23] S. Mukhopadhyay, G.C. Layek, Sk.A. Samad, Study of MHD boundary layer flow over a heated stretching sheet with variable viscosity. Int. J. Heat Mass Transfer 48 (2005) 4460–4466.
[24] I. Pop, R.S.R. Gorla, M. Rashidi, The effect of variable viscosity on flow and heat transfer to a continuous moving flat plate. Int. J. Eng. Sci. 30 (1992) 1–6.
[25] E.M.A. Elbashbeshy, M.A.A. Bazid, The effect of temperature dependent viscosity on heat transfer over a continuous moving surface. J. Phys. D: Appl. Phys. 33 (2000) 2716–2721.
[26] M.S. Alam, M.M. Rahman, M.A. Samad, Transient magnetohydrodynamic free convective heat and mass transfer flow with thermophoresis past a radiate inclined permeable plate in the presence of variable chemical reaction and temperature dependent viscosity, Nonlin. Analy. Model. Control 14 (2009) 3–20.
[27] T.C. Chiam, Heat transfer with variable conductivity in a stagnation-point flow towards a stretching sheet. Int. Commun. Heat Mass Transfer 23 (1996) 239–248.
[28] T.C. Chiam, Heat transfer in a fluid with variable thermal conductivity over a linearly stretching sheet. Acta Mech. 129 (1998) 63–72.
[29] P.S. Datti, K.V. Prasad, M.S. Abel, A. Joshi, MHD visco-elastic fluid flow over a non-isothermal stretching sheet. Int. J. Eng. Sci. 42 (2004) 935–946.
[30] K.V. Prasad, M.S. Abel, S.K. Khan, Momentum and heat transfer in visco-elastic fluid flow in a porous medium over a non-isothermal stretching sheet. Int. J. Numer. Meth. Heat Fluid Flow 10 (2000) 786–802.
[31] M.S. Abel, K.V. Prasad, M. Ali, Buoyancy force and thermal radiation effects in MHD boundary layer visco-elastic fluid flow over continuously moving stretching surface. Int. J. Therm. Sci. 44 (2005) 465–476.
[32] K.V. Prasad, K. Vajravelu, Heat transfer in the MHD flow of a power law fluid over a non-isothermal stretching sheet. Int. J. Heat Mass Transfer 52 (2009) 4956–4965.
[33] K.V. Prasad, D. Pal, V. Umesh, N.S. Prasanna Rao, The effect of variable viscosity on MHD viscoelastic fluid flow and heat transfer over a stretching sheet. Commun. Nonlinear. Sci. Numer. Simulat. 15 (2010) 331–334.
[34] M.M. Rahman, K.M. Salahuddin, Study of hydromagnetic heat and mass transfer flow over an inclined heated surface with variable viscosity and electric conductivity. Commun. Nonlinear. Sci. Numer. Simulat. (2009). doi:10.1016/j.cnsns.2009.08.012.

[35] M.M. Rahman, M.A. Rahman, M.A. Samad, M.S. Alam, Heat transfer in micropolar fluid along a non-linear stretching sheet with temperature dependent viscosity and variable surface temperature. Int. J. Thermophys. 30 (2009) 1649–1670.
[36] M.M. Rahman, M.J. Uddin, A. Aziz, Effects of variable electric conductivity and non-uniform heat source (or sink) on convective micropolar fluid flow along an inclined flat plate with surface. Int. J. Thermal Sci. 48 (2009) 2331–2340.
[37] E.M. Abo-Eldahab, M.A. El-Aziz, Blowing/suction on hydromagnetic heat transfer by mixed convection from an inclined continuously stretching surface with internal heat generation/absorption. Intl. J. Thermal Sci. 43 (2004) 709–719.
[38] K.A. Helmy, MHD boundary layer equations for power law fluids with variable electric conductivity. Meccanica 30 (1995) 187–200.
[39] W.A. Aissa, A.A. Mohammadein, Joule heating effects in a micropolar fluid past a stretching sheet with variable electric conductivity. J. Comput. Appl. Mech. 6 (2005) 3–13.
[40] S.K. Jena, M.N. Mathur, Similarity solution for laminar free convection flow of thermo-micropolar fluid past a non-isothermal vertical flat plate. Int. J. Eng. Sci. 19 (1981) 1431–1439.
[41] G. Ahmadi, Self-similar solution of incompressible micropolar boundary layer flow over a semi-infinite plate. Int. J. Eng. Sci. 14 (1976) 639–646.
[42] J. Peddison, R.P. McNitt, Boundary layer theory for micropolar fluid. Recent Adv. Eng. Sci. 5 (1970) 405–426.
[43] J.X. Ling, A. Dybbs, Forced convection over a flat plate submersed in a porous medium: variable viscosity case, ASME, Paper 87-WA/HT-23, ASME winter annual meeting, Boston, Massachusetts, 13–18, 1987.
[44] R.C. Weast, CRC Handbook of Chemistry and Physics, seventy first ed. CRC Press, Boca Raton, Florida, 1990.
[45] D. Knezevic, V. Savic, Mathematical modeling of changing of dynamical viscosity, as a function of temperature and pressure, of mineral oils for hydraulic systems. Facta. Uni. (Ser. Mech. Eng. 6 (2006) 27–34.
[46] M. Yurusov, M. Pakdemirli, Approximate analytical solutions for the flow of a third-grade fluid in a pipe. Int. J. Non-linear Mech. 37 (2002) 187–195.
[47] T.A. Savvas, N.C. Markatos, C.D. Papaspyrides, On the flow of non-Newtonian polymer solutions. Appl. Math. Model. 18 (1994) 14–22.
[48] A. Pantokratoras, Laminar free-convection over a vertical isothermal plate with uniform blowing or suction in water with variable physical properties. Int. J. Heat Mass Transfer 45 (2002) 963–977.
[49] A. Pantokratoras, Further results on the variable viscosity on flow and heat transfer to a continuous moving flat plate. Int. J. Eng. Sci. 42 (2004) 1891–1896.
[50] P.R. Nachtsheim, P. Swigert, Satisfaction of the asymptotic boundary conditions in numerical solution of the system of non linear equations of boundary layer type. NASA TND-3004 (1965).